

Exotic dark matter search with the MAJORANA DEMONSTRATOR

I.J. Arnquist,¹ F.T. Avignone III,^{2,3} A.S. Barabash,⁴ C.J. Barton,⁵ K.H. Bhimani,^{6,7} E. Blalock,^{8,7} B. Bos,^{6,7} M. Busch,^{9,7} M. Buuck,^{10, a} T.S. Caldwell,^{6,7} Y-D. Chan,¹¹ C.D. Christofferson,¹² P.-H. Chu,¹³ M.L. Clark,^{6,7} C. Cuesta,¹⁴ J.A. Detwiler,¹⁰ Yu. Efremenko,^{15,3} H. Ejiri,¹⁶ S.R. Elliott,¹³ G.K. Giovanetti,¹⁷ M.P. Green,^{8,7,3} J. Gruszko,^{6,7} I.S. Guinn,^{6,7} V.E. Guiseppe,³ C.R. Haufe,^{6,7} R. Henning,^{6,7} D. Hervas Aguilar,^{6,7} E.W. Hoppe,¹ A. Hostiuc,¹⁰ M.F. Kidd,¹⁸ I. Kim,^{13, b} R.T. Kouzes,¹ T.E. Lannen V,² A. Li,^{6,7} A.M. Lopez,¹⁵ J.M. López-Castaño,³ E.L. Martin,^{6,7, c} R.D. Martin,¹⁹ R. Massarczyk,¹³ S.J. Meijer,¹³ S. Mertens,^{20,21} T.K. Oli,⁵ G. Othman,^{6,7, d} L.S. Paudel,⁵ W. Pettus,^{22,23} A.W.P. Poon,¹¹ D.C. Radford,³ A.L. Reine,^{6,7} K. Rielage,¹³ N.W. Ruof,¹⁰ D.C. Schaper,¹³ D. Tedeschi,² R.L. Varner,³ S. Vasilyev,²⁴ J.F. Wilkerson,^{6,7,3} C. Wiseman,^{10, e} W. Xu,⁵ C.-H. Yu,³ and B.X. Zhu^{13, f}

(MAJORANA Collaboration)

¹*Pacific Northwest National Laboratory, Richland, WA 99354, USA*

²*Department of Physics and Astronomy, University of South Carolina, Columbia, SC 29208, USA*

³*Oak Ridge National Laboratory, Oak Ridge, TN 37830, USA*

⁴*National Research Center “Kurchatov Institute” Institute for Theoretical and Experimental Physics, Moscow, 117218 Russia*

⁵*Department of Physics, University of South Dakota, Vermillion, SD 57069, USA*

⁶*Department of Physics and Astronomy, University of North Carolina, Chapel Hill, NC 27514, USA*

⁷*Triangle Universities Nuclear Laboratory, Durham, NC 27708, USA*

⁸*Department of Physics, North Carolina State University, Raleigh, NC 27695, USA*

⁹*Department of Physics, Duke University, Durham, NC 27708, USA*

¹⁰*Center for Experimental Nuclear Physics and Astrophysics, and*

Department of Physics, University of Washington, Seattle, WA 98195, USA

¹¹*Nuclear Science Division, Lawrence Berkeley National Laboratory, Berkeley, CA 94720, USA*

¹²*South Dakota Mines, Rapid City, SD 57701, USA*

¹³*Los Alamos National Laboratory, Los Alamos, NM 87545, USA*

¹⁴*Centro de Investigaciones Energéticas, Medioambientales y Tecnológicas, CIEMAT 28040, Madrid, Spain*

¹⁵*Department of Physics and Astronomy, University of Tennessee, Knoxville, TN 37916, USA*

¹⁶*Research Center for Nuclear Physics, Osaka University, Ibaraki, Osaka 567-0047, Japan*

¹⁷*Physics Department, Williams College, Williamstown, MA 01267, USA*

¹⁸*Tennessee Tech University, Cookeville, TN 38505, USA*

¹⁹*Department of Physics, Engineering Physics and Astronomy, Queen’s University, Kingston, ON K7L 3N6, Canada*

²⁰*Max-Planck-Institut für Physik, München, 80805, Germany*

²¹*Physik Department and Excellence Cluster Universe, Technische Universität, München, 85748 Germany*

²²*Department of Physics, Indiana University, Bloomington, IN 47405, USA*

²³*IU Center for Exploration of Energy and Matter, Bloomington, IN 47408, USA*

²⁴*Joint Institute for Nuclear Research, Dubna, 141980 Russia*

(Dated: June 23, 2022)

With excellent energy resolution and ultra-low level radiogenic backgrounds, the high-purity germanium detectors in the MAJORANA DEMONSTRATOR enable searches for several classes of exotic dark matter (DM) models. In this work we report new experimental limits on keV-scale sterile neutrino DM via the transition magnetic moment from conversion to active neutrinos, $\nu_s \rightarrow \nu_a$. We report new limits on fermionic dark matter absorption ($\chi + A \rightarrow \nu + A$) and sub-GeV DM-nucleus $3 \rightarrow 2$ scattering ($\chi + \chi + A \rightarrow \phi + A$), and new exclusion limits for bosonic dark matter (axionlike particles and dark photons). These searches utilize the 1–100 keV low energy region of a 37.5 kg-y exposure collected by the DEMONSTRATOR between May 2016 and Nov. 2019, using a set of ^{76}Ge -enriched detectors whose surface exposure time was carefully controlled, resulting in extremely low levels of cosmogenic activation.

As large-scale dark matter experiments have rejected much of the traditional WIMP parameter space, interest in alternative dark matter models has increased. Popular models include light (sub-GeV) dark matter, axionlike particles (ALP), dark photons, and keV-scale sterile neutrinos. Experimental searches have previously placed limits on bosonic dark matter in the 1–100 keV range

(scalar or axionlike particles and vector or dark photons) [1, 2], with the most stringent limits to date on the scalar and vector couplings set by XENON1T [3]. GERDA has set limits up to 1 MeV [4], while DAMIC has achieved the lowest electron recoil energy thresholds of 200 eV [5], and nuclear-recoil detectors such as CRESST have achieved sensitivity to nuclear recoil ionization to

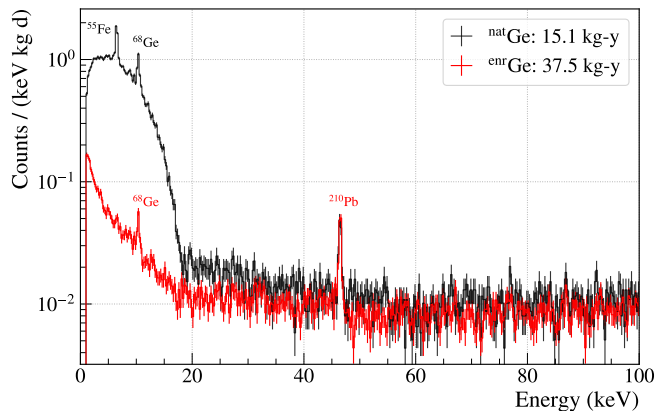


FIG. 1. Energy spectra from $^{\text{nat}}\text{Ge}$ and $^{\text{enr}}\text{Ge}$ HPGe detectors, with a 1 keV lower threshold. The spectrum in the $^{\text{nat}}\text{Ge}$ below 20 keV is tritium-dominated. Lower levels of tritium, ^{55}Fe , ^{65}Zn , ^{68}Ge show that surface exposure control of the $^{\text{enr}}\text{Ge}$ material significantly reduced cosmogenic activation. The ^{65}Zn contribution at 9.0 keV is small but nonzero, and can be seen in Fig. 3. The average $^{\text{enr}}\text{Ge}$ count rate is 0.011 ± 0.002 counts/(keV kg d) in the 20–40 keV range.

30 eV [6]. Recently, interest has increased in fermionic dark matter, which may convert to neutrinos upon interaction with a target [7–10]. A low-background detector array with excellent energy resolution [11] is an ideal environment to search for rare peaks from several exotic DM models.

The MAJORANA DEMONSTRATOR conducted a search for neutrinoless double-beta decay ($\beta\beta(0\nu)$) from 2015 to 2019 with a 29.7-kg set of ^{76}Ge -enriched high-purity germanium (HPGe) p-type point contact (PPC) detectors manufactured by AMETEK-ORTEC [12, 13], at the 4850' level of the Sanford Underground Research Facility in Lead, South Dakota [14, 15]. In 2020 a set of inverted-coaxial PPC detectors were swapped in for evaluation prior to use in the LEGEND-200 experiment [16]. A final exposure of ~ 65 kg-y was collected before all $^{\text{enr}}\text{Ge}$ detectors were removed in 2021 for installation in the LEGEND-200 experiment. The DEMONSTRATOR continues to operate with 14.3 kg of natural-abundance Ge detectors for background studies and other rare-event searches.

From the primary data taking period, 37.5 kg-y $^{\text{enr}}\text{Ge}$ and 15.1 kg-y $^{\text{nat}}\text{Ge}$ exposure were selected for an exotic dark matter analysis in the lowest-energy region of the spectrum, 1–100 keV. The energy estimator, time-dependent detector selection, and muon veto cut are computed in the $\beta\beta(0\nu)$ analysis, and additional low energy pulse shape parameters are computed for data cleaning and surface event rejection. An event multiplicity cut is applied to select only single-detector events. The DM-matter interaction cross-section for all models considered here is known to be extremely small, and the probability of DM multiple-scattering in the detector array is negli-

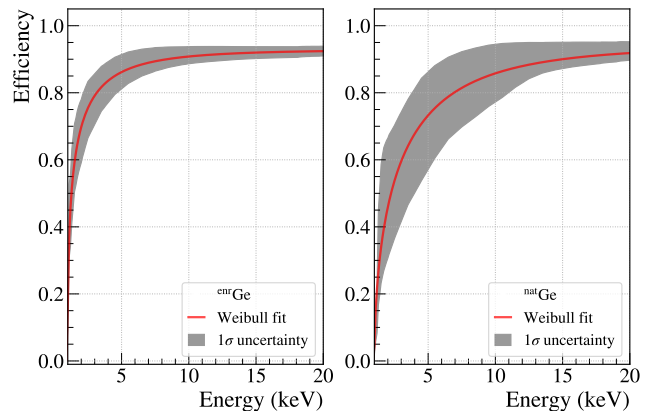


FIG. 2. Total efficiency and uncertainty for $^{\text{enr}}\text{Ge}$ and $^{\text{nat}}\text{Ge}$ detectors. A fit to a cumulative Weibull distribution (red) gives the central value, while the gray region gives the data-driven 1σ uncertainty, with contributions from changing energy thresholds and pulse shape analysis cuts.

ble for this exposure. Multi-detector events from lightly ionizing particles (LIPs) were searched for in Ref. [17]. A technical paper with additional details on the low energy data cleaning and efficiency determination is in preparation.

The surface exposure of the $^{\text{enr}}\text{Ge}$ detectors was carefully limited during fabrication and storage, resulting in the lowest cosmogenic activation of any Ge experiment to date and increased sensitivity to low-statistics rare events. Since the surface exposure time of the $^{\text{nat}}\text{Ge}$ detectors was not limited, they show a strong tritium feature and associated cosmogenic lines, while the $^{\text{enr}}\text{Ge}$ detectors show significantly reduced ^{68}Ge , ^{65}Zn , and tritium. Fig 1 gives the energy spectrum of the $^{\text{enr}}\text{Ge}$ and $^{\text{nat}}\text{Ge}$ detectors used in this analysis after data cleaning.

Energy-degraded events near the millimeter-thick Ge(Li) n^+ detector surfaces are known to produce pulses with a slower rising edge that may be rejected by pulse shape analysis [18]. Our algorithm fits each wavelet-denoised waveform to a sigmoid function, giving pulse shape rejection capability to 1 keV, similar to Ref. [19]. The turnover of the $^{\text{nat}}\text{Ge}$ spectrum at energies below 5 keV shows the successful rejection of slow pulse signals by the data cleaning algorithm. The $^{\text{enr}}\text{Ge}$ spectrum shows a rising spectral shape below 10 keV which persists after aggressive slow pulse cuts, indicating the excess signal is dominated by fast events. These may originate from ionization in the main fiducial (bulk) volume, events near the p^+ contact, or from the micrometer-thick amorphous Ge passivation layer for the PPC detector geometry [20]. Despite detector storage in nitrogen environments, residual contamination of the detector component surfaces by long-lived Rn progeny including ^{210}Pb , ^{210}Bi , and ^{210}Po plausibly explain the signal. We observe the 46.5 keV peak from ^{210}Pb at the same intensity in both sets of detectors, indicating roughly uniform

distribution of the source in the array, but notably do not observe the associated 10.8 keV line, which may not penetrate the passivated surface region. Low energy β emission from this decay chain is also expected, which may penetrate the region and cause the rise.

The signal acceptance efficiency of the pulse shape analysis cuts is computed by considering the time-dependent detector energy thresholds, and the detector-specific efficiency of the n^+ slow pulse cut. This is determined from weekly ^{228}Th calibration data using the 238.6 keV line from ^{212}Pb , which is not emitted in coincidence with other gamma rays. Paired detector events with sum energy ~ 239 keV are likely to include a small-angle Compton scatter in the first detector, which can deposit as little as 1 keV with a mean free path of 14 mm, well into the bulk region. The combined efficiency for $^{\text{enr}}\text{Ge}$ and $^{\text{nat}}\text{Ge}$ detectors is given in Fig. 2, and each is fit to the cumulative distribution of a Weibull function, a heuristic choice of an asymmetric function [21]. The fit constants (*shape, location, scale, amplitude*) are (0.4633, 0.9866, 0.4960, 0.9283) for the $^{\text{enr}}\text{Ge}$ and (0.5922, 0.9880, 1.9911, 0.9394) for the $^{\text{nat}}\text{Ge}$ detectors. The efficiency in the $^{\text{enr}}\text{Ge}$ is 15.9% at 1 keV, rising to 79.1% at 3 keV.

In this Letter, we give exclusion limits for several classes of DM models using the 37.5 kg-y exposure obtained from the $^{\text{enr}}\text{Ge}$ detectors in the DEMONSTRATOR. The models considered here are expected to produce a sharp peak with a width close to the expected energy resolution, $\sigma_D(E)$ [15]. We scan for a peak at energies E_i between 1–100 keV, sampling at intervals proportional to half the expected detector energy resolution, ranging from 0.15 keV FWHM at 1 keV to 0.23 keV at 100 keV, taking a 30% resolution uncertainty based on studies of cosmogenic and ^{228}Th calibration peak widths. At each energy we evaluate the maximum possible counts attributable to a rare signal, N_U . To set an upper limit on the various couplings of interest at each E_i , we perform an unbinned extended maximum likelihood fit in a $\pm(7\sigma_D + 1)$ keV window, weighting the counts by the analytic cut efficiency and its uncertainty shown in Fig. 2. We profile the likelihood function to a 90% confidence level (CL) to identify any excess in the number of counts at each peak location, and we find no significant peak-like excess in the 1–100 keV region that do not originate from known backgrounds. The total probability density function \mathcal{P} used for each local spectrum model at E_i is given by

$$\mathcal{P}(E_i) = n_0 \mathcal{P}_{\text{pol}2} + \sum_{n_{\text{pks}}} n_i \mathcal{P}_{G,i} + N_U \mathcal{P}_{\text{rare}} \quad (1)$$

where $\mathcal{P}_{\text{rare}}$ are the Gaussian-distributed rare signal peaks at varying energies, and $\mathcal{P}_{G,i}$ are the Gaussian PDFs for known cosmogenic peaks. The yields (counts) n_i are convolved with the cut efficiency and its uncertainty at each energy E_i as Gaussian constraints in each unbinned fit. When the rare peak $\mathcal{P}_{\text{rare}}$ is degenerate

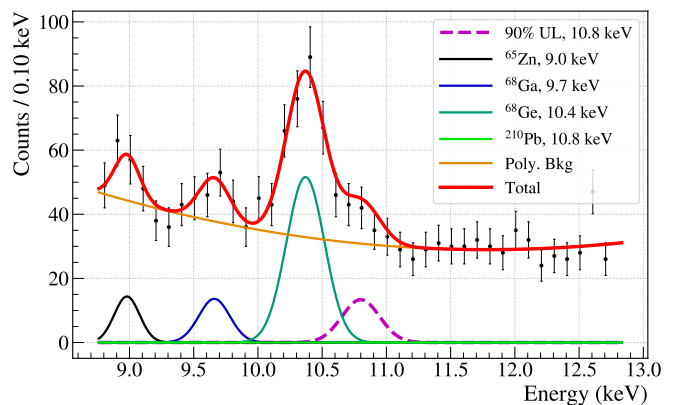


FIG. 3. An example fit to the energy spectrum that provides a calculation of the 90% UL for a rare peak at 10.8 keV, where a ^{210}Pb line is possible but not seen. Initial guesses for the cosmogenic yields are taken from a preliminary fit without the signal peak. When the signal peak has any overlap with a cosmogenic line, the cosmogenic heights are minimized to maximize N_U .

with a known cosmogenic line, N_U is constrained to include the full yield n_i at the peak. $\mathcal{P}_{\text{poly}}$ is a second-order Chebyshev polynomial estimation for the continuum shape in each fit window. This heuristic choice assigns the least strength to background counts in the window, and requires only an initial guess for the yields n_i . The expected number of detected counts at energy E for a mass m_χ is given by

$$\frac{dN}{dE} = \Phi_{\text{DM}}(m_\chi) \sigma(m_\chi) \eta(E) \mathcal{P}_{\text{rare}}(E) MT \frac{m_{\text{enr}}}{m_{\text{nat}}} \quad (2)$$

Here, Φ_{DM} is the dark matter flux, the exposure MT is in kg-y, and the detection efficiency $\eta(E)$ is convolved with the rare signal peak $\mathcal{P}_{\text{rare}}$. The rate is weighted by the relative molecular weights of the $^{\text{enr}}\text{Ge}$ detectors (75.668 ± 0.010 g/mol) to the standard weight of $^{\text{nat}}\text{Ge}$, 72.63 g/mol. The interaction cross-section σ varies with the DM model of interest. An example calculation of N_U at 10.8 keV is shown in Fig. 3.

Sterile neutrino transition magnetic moment.— Sterile neutrinos have been proposed as a cold (nonrelativistic) DM candidate [22–27], capable of producing a detectable upscattering event in a DM detector. The nonzero mass of the neutrino allows radiative decay between states [28], including transitions of heavy right-handed sterile neutrinos ν_s with keV-MeV scale masses into active $\nu_a = \nu_{e,\mu,\tau}$. Radiative decay of a 7.1 keV DM ν_s may explain anomalous X-ray emission lines at ~ 3.5 keV observed by the XMM-Newton space observatory [29, 30], though the explanation is contested [31].

Current best limits on any neutrino transition magnetic moment (TMM) from active-to-sterile conversion come from solar neutrino-electron scattering in Borexino ($\nu_\mu \rightarrow \nu_s$), with the best limit $\mu_{\mu s} < 7 \times 10^{-11} \mu_B$ for ster-

ile neutrino masses 10–100 keV [32]. Flavor-dependent couplings have been proposed to avoid constraints from supernova SN1987A and the CMB [33, 34]. An active-to-sterile transition ($\nu_a \rightarrow \nu_s$) from incident solar neutrinos via TMM may also account for the excess of events below 5 keV observed by XENON1T [35, 36]. While this interpretation does not depend on any DM assumption on ν_s , a limit on μ_{sa} can impact both the XENON1T excess interpretation and the dark matter sterile neutrino hypothesis.

We consider the atomic ionization process by incoming sterile neutrinos $\nu_s + A \rightarrow \nu_a + A^+ + e^-$. In this process, the limit on the 4-momentum transfer $q^2 \rightarrow 0$ is kinematically accessible due to the two-body atomic final state of the positive ion plus the ionization electron [37]. Near this limit, the atomic ionization process can be viewed as a two-step process, where the exchange photon emitted from the incoming ν_s interacts coherently with an atom in the detector target, producing ionization. The singularity due to the real photon pole in the interaction cross section is accessed, and the cross section is enhanced by orders of magnitude at the energy transfer $T = m_s/2$, half the mass of the sterile neutrino [37]. This would produce a peak-like signature in the energy spectrum. Considering this resonance in presence of a rich ν_s source allows more stringent limits to be set on μ_{sa} than previous limits from solar neutrino-electron scattering [37]. In this analysis, we assume that the local DM halo consists of ν_s , for comparison with Ref. [37]¹.

Near the resonant energy $E = m_s/2$, the equivalent photon approximation (EPA) becomes valid [37]. Within the interval $E = m_s/2 \pm |\vec{k}_s|/2$, where \vec{k}_s is the sterile neutrino momentum vector, the amplified differential cross section has the form

$$\frac{d\sigma(m_s, v)}{dE} \approx \left(\frac{\mu_{sa}}{2m_e}\right)^2 \frac{\alpha}{2n_A} \frac{m_s^2}{|v|^2}, \quad (3)$$

where α is the electromagnetic fine structure constant, n_A is the number density of Ge atoms and v is the velocity of the incoming sterile neutrino. As a consequence, a peaked signature at $E = m_s/2$ is expected. With Eq. 3, we can set a limit on μ_{sa} in terms of the incoming sterile neutrino flux at any value of m_s . For any dark matter model, the DM interaction rate per unit mass in a terrestrial detector with isotopic mass m_A can be calculated by

$$\frac{dR}{dE} = \frac{\rho_\chi}{m_\chi m_A} \int_{u_{\min}}^{\infty} \left[\frac{d\sigma(m_s, \vec{u})}{dE} u f(\vec{u}) \right] d^3u \quad (4)$$

¹ The original μ_{sa} limit using the same postulate in Ref. [37] was found to be erroneous by a factor 14, which has been taken into account in Fig. 4. An erratum is in preparation by the authors [38].

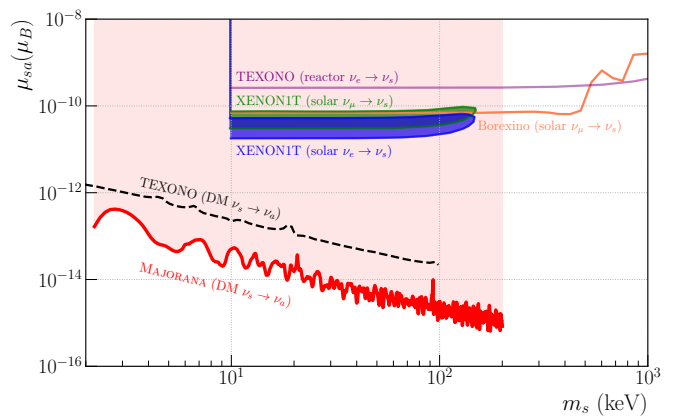


FIG. 4. The 90% limit on the sterile neutrino transition magnetic moment via atomic ionization from MAJORANA (red), under the assumption of the DM sterile neutrinos. Our result implies that the sterile neutrino TMM interpretation of the XENON1T excess is inconsistent with the DM sterile neutrino hypothesis.

where $\vec{u} = \vec{v} + \vec{v}_e$ is the velocity of the dark matter in the Earth’s reference frame, \vec{v} is the velocity of the dark matter in the Galactic rest frame, $\vec{v}_e = \vec{v}_e(t)$ is the circular motion of the Earth in the Galactic frame, u_{\min} is the minimum speed of the DM to produce detectable recoil and $f(\vec{u})$ is the DM velocity distribution in the Earth’s reference frame. If the sterile neutrinos are taken as a DM candidate, $m_\chi = m_s$, and the standard local DM density $\rho_\chi = 0.4 \text{ GeV/cm}^3$.

We use a property of the EPA cross section, which has a plateau at $E = m_e/2$ with u^{-2} -dependent height and u -dependent width. All u -dependence in the integrand of Eq. 4 is cancelled except $f(\vec{u})$, which integrates to unity by definition. The expression for the event rate R is independent of the specific DM velocity distribution.

With the EPA differential cross section at the resonant energy and setting $u_{\min} = 0$ for inelastic scattering, Eq. 4 can be integrated to get an expression of R , and set equal to the experimental upper limit:

$$R = \frac{\rho_\chi \mu_{sa}^2 \alpha m_s^2}{m_A 4m_e^2 2n_A} = \frac{N_U}{MT} \quad (5)$$

Our limit on μ_{sa} is compared to the μ_{sa} limits from TEXONO and Borexino neutrino experiments in Fig. 4. The parameter spaces expected to cause the XENON1T excess are also illustrated. Note that other active-to-sterile transition searches do not necessarily make any assumption of sterile neutrino dark matter. Our result implies that if the DM halo is assumed to consist of keV-scale sterile neutrinos, the value of μ_{sa} is too low to produce the excess of events observed by XENON1T.

Fermionic DM.— Recent papers have discussed fermionic DM-neutrino interactions, modeled as a Yukawa-like interaction with a bosonic mediator [7–9, 39]. In the presence of this mediator, fermionic DM

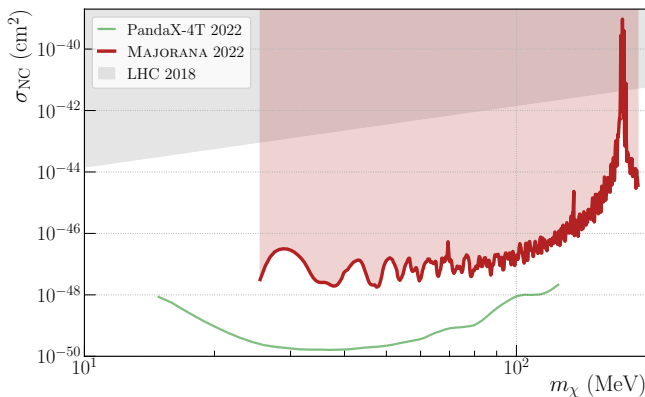


FIG. 5. 90% exclusion limit for the $\chi + A \rightarrow \nu + A$ fermionic DM absorption process. Previous constraints from LHC Z_0 monojet searches are shown in gray. The Helm form factor for Ge determines the overall shape of the curve, and contains a pole which produces the peak-like structure at 174 MeV [41, 42].

can scatter off a nucleus A and convert to standard model neutrinos via the $2 \rightarrow 2$ neutral-current (NC) interaction $\chi + A \rightarrow \nu + A$. If the incoming DM is non-relativistic, the signature of this inelastic scattering is a monoenergetic peak at the nuclear recoil energy $E_R \simeq m_\chi^2/2M_T$, where M_T is the isotopic mass of the target. The total absorption rate is given by

$$\frac{N_U}{MT} = \frac{\rho_\chi}{m_\chi} \sigma_{\text{NC}} \sum_j N_{A_j} A_j^2 F_j(m_\chi)^2 \Theta(E_{R,j} - E_{\text{th}}). \quad (6)$$

The main quantity of interest is the DM-nucleon scattering cross section σ_{NC} . The local DM density is taken to be $\rho_{\text{DM}} = 0.4 \text{ GeV/cm}^3$ as in Ref. [40]. The sum over target nuclei j is performed over the five most abundant Ge isotopes in the $^{\text{enr}}\text{Ge}$ detectors. N_{A_j} is the number of nuclei for each isotope with mass number A_j , and $F_j(m_\chi)$ is the normalized Helm form factor [41, 42] evaluated at momentum transfer $q = m_\chi$ for non-relativistic incoming DM. The step function Θ is the experimental energy threshold E_{th} and represents the nuclear recoil energy threshold for detectable signals.

A quenching factor for germanium must also be applied to convert the observed electron equivalent ionization (keVee) to the energy of the nuclear recoil E_R (keVnr) [43–45]. To describe the stopping of few-keV ions in Ge at $\sim 77 \text{ K}$, we select the quenching factor $Q = 0.2(E_{\text{nr}}/\text{keVnr})^{1.12}$ suggested by CoGeNT [18], as most applicable to the 1–100 keV energy range [43, 46, 47]. For energies above 1 keVee, there is little dependence on the choice of quenching factor, and the Lindhard model is adequate. At 1 keVee, our nuclear recoil threshold is $E_{\text{nr}} = 4.5 \text{ keVnr}$, corresponding to a fermionic DM mass of $m_\chi = 25.5 \text{ MeV}$.

Only two other searches for fermionic dark matter have been performed to date. Z_0 monojet searches at the LHC

provided indirect constraints [48], and very recently PandaX released a search using 0.63 ton-yr of exposure from the PandaX-4T detector [10]. Our search for fermionic dark matter, shown in Fig. 5 is the first done with a Ge array, surpassing the Z_0 monojet constraints by roughly five orders of magnitude, but is surpassed by the PandaX-4T result due to the significantly larger exposure. Our result is the first to set experimental bounds above masses of 120 MeV. A larger-scale future Ge array with backgrounds comparable to MAJORANA could be competitive with the Xe results. We find a best 90% upper limit on the DM-nucleon coupling $\sigma_{\text{NC}} < 1.620 \times 10^{-48} \text{ cm}^2$ at a DM mass of 48.07 MeV.

Sub-GeV DM-nucleus $3 \rightarrow 2$ scattering.— Recent work has shown that the detection probability of observing DM-nucleus interactions in Ge would be significantly enhanced for sub-GeV DM if the $3 \rightarrow 2$ process $\chi + \chi + A \rightarrow \phi + A$ is considered [49]. The signature of this process is an absorption peak at the nuclear recoil energy $E_R \simeq (4 - \xi^2)m_\chi^2/2M_T$, where ξ is the mass ratio of the final and initial dark matter states ϕ and χ , and M_T is the isotopic mass of the target. The value of ξ is model-dependent, and is 0 for a massless (dark photon) final state. For a bound DM final state, it is obtained by $\xi = (2m_\chi + \epsilon_1)/m_\chi$, where the binding energy is $\epsilon_1 = -(g_D^4 m_\chi)/(64\pi^2)$ and g_D is the new gauge coupling [50]. Setting the gauge coupling $|g_D| = 3$ for the bound state DM as in Ref. [49], we obtain $\xi = 1.87$ for the bound final state.

The total rate of nuclear recoil events has a similar form to the fermionic DM absorption (Eq. 6):

$$\frac{N_U}{MT} = \left(\frac{\rho_\chi}{m_\chi}\right)^2 \langle \sigma_{\text{NC}}^{3 \rightarrow 2} v^2 \rangle \times \sum_j N_{A_j} A_j^2 F_j(q)^2 \Theta(E_{R,j} - E_{\text{th}}) \quad (7)$$

where $\langle \sigma_{\text{NC}}^{3 \rightarrow 2} v \rangle$ is the average three-body inelastic cross section per nucleon with the initial DM velocity v .

This search is the first to set an experimental limit for this $3 \rightarrow 2$ scattering process. We place our limit on the $(m_\chi, \sigma_{\text{NC}}^{3 \rightarrow 2} v^2 n_\chi)$ parameter as suggested in Ref. [49], where $n_\chi = \rho_\chi/m_\chi$ is the DM number density. The 90% exclusion curves are shown in Fig. 6. For the massless final state, the best limit on the coupling is $\langle \sigma_{\text{NC}}^{3 \rightarrow 2} v^2 \rangle n_\chi < 4.570 \times 10^{-48} \text{ cm}^2$, at a mass of 24.04 MeV. For the bound final state, we find a best limit of $1.297 \times 10^{-47} \text{ cm}^2$ at a DM mass of 68.22 MeV.

Bosonic DM.— Several experiments have searched for both pseudoscalar (axionlike) and vector (dark photon) bosonic dark matter as an alternative to WIMP models. These are non-relativistic DM candidates whose mass energy is absorbed by a target atom through a variation of the photoelectric (or axioelectric) effect [1, 51, 52], producing a peak at the rest mass energy. For axionlike particles, we assume a DM density $\rho_{\text{DM}} = 0.3 \text{ GeV cm}^{-3}$,

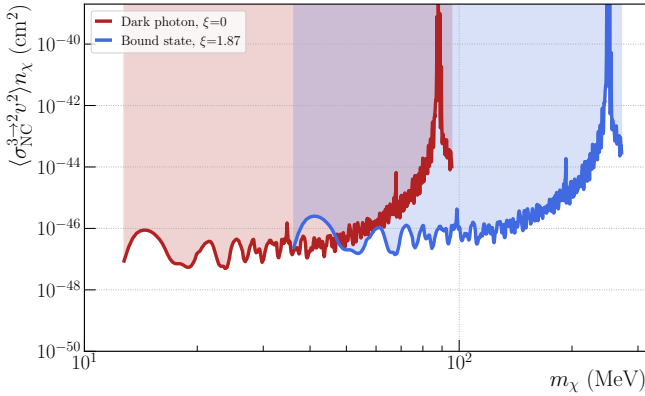


FIG. 6. 90% exclusion limit for the DM-nucleus 3-2 inelastic scattering process, $\chi + \chi + A \rightarrow \phi + A$. $\xi = 0$ is a massless dark photon final state and $\xi = 1.87$ is a bound final state.

and a DM velocity such that the energy is approximately equal to its mass, $\beta = v_{\chi}/c = 0.001$. This follows standard assumptions in Refs. [1, 2, 4], defining m_{χ} as the rest mass in keV. The DM flux ($\text{cm}^{-2} \text{d}^{-1}$) becomes

$$\Phi_{\text{DM}} = \frac{\rho_{\text{DM}} v_{\chi}}{m_{\chi}} = \frac{7.8 \times 10^{-17}}{m_{\chi}} \quad (8)$$

The interaction, known as the axioelectric effect [51, 52] has a cross section given by

$$\sigma_{ae}(E) = g_{ae}^2 \frac{E^2 \sigma_{pe}(E)}{\beta} \left(\frac{3}{16\pi\alpha m_e^2} \right) \quad (9)$$

Here, m_e is the electron mass in keV, σ_{pe} is the photoelectric cross section for Ge at E_i [53]. The upper limit on the pseudoscalar coupling g_{ae} can be expressed as follows, factoring it out of σ_{ae} such that $\sigma_{ae} \equiv g_{ae}^2 \sigma'_{ae}$:

$$|g_{ae}| \leq \left(\frac{N_U m_{\chi}}{MT (7.8 \times 10^{17}) \sigma'_{ae}(m_{\chi})} \right)^{1/2} \quad (10)$$

The resulting exclusion plot is shown in Fig. 7.

Recently, Ferreira et. al [54] have argued that the parameter space previously searched by MAJORANA and other experiments is already ruled out since the lifetime of the ALPs would be shorter than the age of the Universe. Our search reaches below 5 keV, surpassing the limits from x-ray and gamma-ray limits on lifetime [54]. In the full energy range, we find a best upper limit on the pseudoscalar axion-electron coupling constant $g_{ae} < 1.425 \times 10^{-13}$ at 17.28 keV, and below 5 keV, a best upper limit of $g_{ae} < 1.542 \times 10^{-13}$ at 2.64 keV. The best limits to date are set by large-scale Xe experiments due to their much larger active mass [3].

For vector bosonic dark matter (dark photons), the coupling constant to electrons α' is related to the electromagnetic fine structure constant α , with experimental limits set on the kinetic mixing $\kappa^2 = \alpha'/\alpha$ or its logarithm. To compute the expected counts, the product of

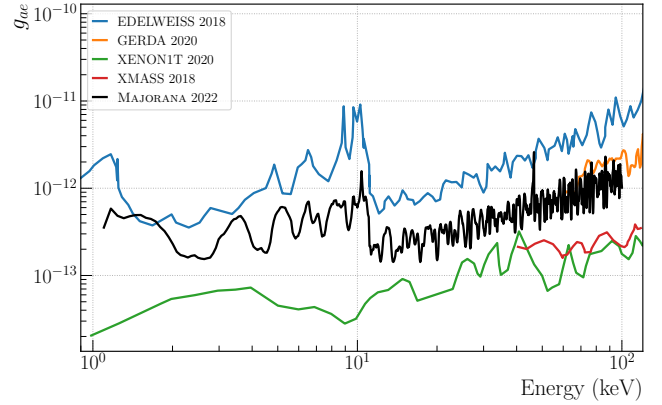


FIG. 7. Exclusion limits for pseudoscalar (axionlike) bosonic dark matter. The MAJORANA curve (black) is the best limit for any Ge experiment, with the increased exposure and a factor 5 reduction in energy threshold from the previous analysis. Xe experiments are capable of tighter limits due to their factor O(10) larger active mass [35, 55].

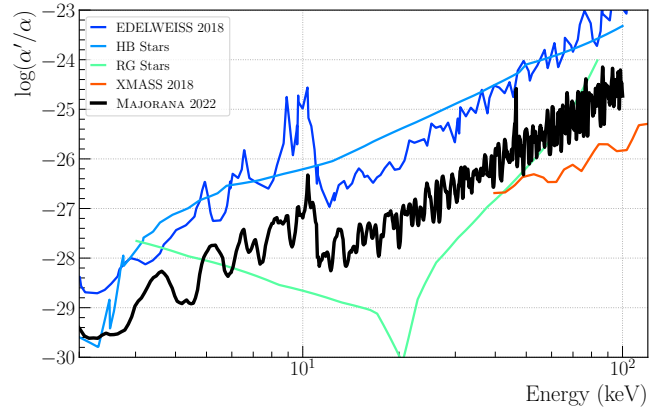


FIG. 8. Exclusion limits for vector bosonic (dark photon) dark matter.

the DM flux and interaction cross section ($\text{kg}^{-1} \text{d}^{-1}$) is replaced by [1]:

$$\Phi_{DM} \sigma_{ve} = \frac{4 \times 10^{23}}{m_{\chi}} \left(\frac{\alpha'}{\alpha} \right) \frac{\sigma_{pe}(m_{\chi})}{A} \quad (11)$$

Searching for a rare peak at each energy E_i as before, we obtain a limit on the coupling as a function of the mass m_{χ} :

$$\frac{\alpha'}{\alpha} \leq \left(\frac{N_U A m_{\chi}}{MT (4 \times 10^{23}) \sigma_{pe}(m_{\nu})} \right) \quad (12)$$

Fig. 8 shows the exclusion plot for the vector DM search. We find a best upper limit on the coupling at 2.29 keV, $\alpha'/\alpha < 2.414 \times 10^{-30}$.

Discussion.— In this Letter we report results of several exotic DM searches using the MAJORANA low energy data set, using a 90% CL profile likelihood method to set an upper limit on counts attributable to rare peaks in the

1–100 keV energy region. Our result indicates that the transition magnetic moment between sterile and active neutrinos is too low to produce the XENON1T excess, if keV-scale ν_s DM is assumed. We set new experimental limits on the $(\chi + A \rightarrow \nu + A)$ inelastic fermionic DM absorption, and sub-GeV DM-nucleus $3 \rightarrow 2$ scattering for both massless and bound final DM states. Our limits for fermionic and bosonic dark matter are currently the best among Ge experiments, while Xe experiments have surpassed this with their significantly larger active mass. Controlling the surface exposure time of the detectors in the DEMONSTRATOR was key to increase statistical sensitivity in the low-energy region. The proposed next-generation $\beta\beta(0\nu)$ LEGEND experiment [16] may be capable of extending the results of the DEMONSTRATOR, with a significantly larger (ton-scale) active mass, lower backgrounds, and equally low energy thresholds. With its final goal of 10 ton-years exposure, significant improvements on the limits presented here may be realized.

This material is based upon work supported by the U.S. Department of Energy, Office of Science, Office of Nuclear Physics under contract / award numbers DE-AC02-05CH11231, DE-AC05-00OR22725, DE-AC05-76RL0130, DE-FG02-97ER41020, DE-FG02-97ER41033, DE-FG02-97ER41041, DE-SC0012612, DE-SC0014445, DE-SC0018060, and LANLEM77/LANLEM78. We acknowledge support from the Particle Astrophysics Program and Nuclear Physics Program of the National Science Foundation through grant numbers MRI-0923142, PHY-1003399, PHY-1102292, PHY-1206314, PHY-1614611, PHY-1812409, PHY-1812356, and PHY-2111140. We gratefully acknowledge the support of the Laboratory Directed Research & Development (LDRD) program at Lawrence Berkeley National Laboratory for this work. We gratefully acknowledge the support of the U.S. Department of Energy through the Los Alamos National Laboratory LDRD Program and through the Pacific Northwest National Laboratory LDRD Program for this work. We gratefully acknowledge the support of the South Dakota Board of Regents Competitive Research Grant. We acknowledge the support of the Natural Sciences and Engineering Research Council of Canada, funding reference number SAPIN-2017-00023, and from the Canada Foundation for Innovation John R. Evans Leaders Fund. This research used resources provided by the Oak Ridge Leadership Computing Facility at Oak Ridge National Laboratory and by the National Energy Research Scientific Computing Center, a U.S. Department of Energy Office of Science User Facility located at Lawrence Berkeley National Laboratory. We thank our hosts and colleagues at the Sanford Underground Research Facility for their support.

- ^a Present address: SLAC National Accelerator Laboratory, Menlo Park, CA 94025, USA
- ^b inwookkim@lanl.gov
- ^c Present address: Duke University, Durham, NC 27708
- ^d Present address: Universität Hamburg, Institut für Experimentalphysik, Hamburg, Germany
- ^e wisecg@uw.edu
- ^f Present address: Jet Propulsion Laboratory, California Institute of Technology, Pasadena, CA 91109, USA
- [1] M. Pospelov, A. Ritz, and M. Voloshin, *Physical Review D* **78**, 115012 (2008).
- [2] N. Abgrall *et al.*, *Physical Review Letters* **118**, 161801 (2017).
- [3] E. Aprile *et al.* (XENON Collaboration), *Physical Review Letters* **123**, 241803 (2019).
- [4] M. Agostini *et al.* (GERDA Collaboration), *Physical Review Letters* **125**, 011801 (2020).
- [5] A. Aguilar-Arevalo *et al.* (DAMIC Collaboration), *Physical Review Letters* **125**, 241803 (2020).
- [6] A. Abdelhameed *et al.* (CRESST Collaboration), *Physical Review D* **100**, 102002 (2019).
- [7] J. A. Dror, G. Elor, and R. McGehee, *Journal of High Energy Physics* **2020**, 1 (2020).
- [8] J. A. Dror, G. Elor, and R. McGehee, *Phys. Rev. Lett.* **124**, 181301 (2020).
- [9] J. A. Dror, G. Elor, R. McGehee, and T.-T. Yu, *Phys. Rev. D* **103**, 035001 (2021).
- [10] L. Gu *et al.* (PandaX Collaboration), arXiv preprint arXiv:2205.15771 (2022).
- [11] N. Abgrall *et al.* (MAJORANA Collaboration), *Journal of Instrumentation* **17**, T05003 (2022).
- [12] P. S. Barbeau, J. I. Collar, and O. Tench, *Journal of Cosmology and Astroparticle Physics* **2007**, 009 (2007).
- [13] N. Abgrall *et al.* (MAJORANA Collaboration), *NIM A* **877**, 314 (2018).
- [14] C. Aalseth, *et al.* (MAJORANA Collaboration), *Physical Review Letters* **120**, 132502 (2018).
- [15] S. Alvis *et al.* (MAJORANA Collaboration), *Physical Review C* **100**, 025501 (2019).
- [16] N. Abgrall *et al.* (LEGEND Collaboration), arXiv preprint arXiv:2107.11462 (2021).
- [17] S. Alvis *et al.* (Majorana Collaboration), *Phys. Rev. Lett.* **120**, 211804 (2018).
- [18] C. E. Aalseth *et al.* (CoGeNT Collaboration), *Phys. Rev. D* **88**, 012002 (2013).
- [19] L. Yang *et al.*, *NIM A* **886**, 13 (2018).
- [20] R. Li *et al.*, arXiv preprint arXiv:2201.02961 (2022).
- [21] “Scipy, `scipy.stats.weibull_min`,” https://docs.scipy.org/doc/scipy/reference/generated/scipy.stats.weibull_min.html, accessed: 2018-06-11.
- [22] S. Dodelson and L. M. Widrow, *Phys. Rev. Lett.* **72**, 17 (1994).
- [23] X. Shi and G. M. Fuller, *Phys. Rev. Lett.* **82**, 2832 (1999).
- [24] K. Abazajian, G. M. Fuller, and M. Patel, *Phys. Rev. D* **64**, 023501 (2001).
- [25] A. Dolgov and S. Hansen, *Astroparticle Physics* **16**, 339 (2002).
- [26] T. Asaka and M. Shaposhnikov, *Physics Letters B* **620**, 17 (2005).
- [27] L. Canetti, M. Drewes, T. Frossard, and M. Shaposhnikov, *Phys. Rev. D* **87**, 093006 (2013).

- [28] P. B. Pal and L. Wolfenstein, *Physical Review D* **25**, 766 (1982).
- [29] E. Bulbul, M. Markevitch, A. Foster, R. K. Smith, M. Loewenstein, and S. W. Randall, *The Astrophysical Journal* **789**, 13 (2014).
- [30] A. Boyarsky, O. Ruchayskiy, D. Iakubovskiy, and J. Franse, *Phys. Rev. Lett.* **113**, 251301 (2014).
- [31] C. Dessert, N. L. Rodd, and B. R. Safdi, *Science* **367**, 1465 (2020).
- [32] O. Miranda, D. Papoulias, O. Sanders, M. Tórtola, and J. Valle, *Journal of High Energy Physics* **2021**, 1 (2021).
- [33] I. M. Shoemaker, Y.-D. Tsai, and J. Wyenberg, *Phys. Rev. D* **104**, 115026 (2021).
- [34] V. Brdar, A. Greljo, J. Kopp, and T. Opferkuch, *Journal of Cosmology and Astroparticle Physics* **2021**, 039 (2021).
- [35] E. Aprile *et al.* (XENON Collaboration), *Phys. Rev. D* **102**, 072004 (2020).
- [36] O. Miranda, D. Papoulias, M. Tórtola, and J. Valle, *Physics Letters B* **808**, 135685 (2020).
- [37] J.-W. Chen, H.-C. Chi, S.-T. Lin, C.-P. Liu, L. Singh, H. T. Wong, C.-L. Wu, and C.-P. Wu, *Phys. Rev. D* **93**, 093012 (2016).
- [38] I. Kim, J.-W. Chen, and S.-T. Lin, Private Communication (2021).
- [39] N. Hurtado, H. Mir, I. M. Shoemaker, E. Welch, and J. Wyenberg, *Phys. Rev. D* **102**, 015006 (2020).
- [40] P. Fernández de Salas and A. Widmark, *Rep. Prog. Phys* **84**, 104901 (2021).
- [41] R. H. Helm, *Physical Review* **104**, 1466 (1956).
- [42] J. Lewin and P. Smith, *Astroparticle Physics* **6**, 87 (1996).
- [43] D. Barker and D.-M. Mei, *Astroparticle Physics* **38**, 1 (2012).
- [44] D. Barker, W.-Z. Wei, D.-M. Mei, and C. Zhang, *Astroparticle Physics* **48**, 8 (2013).
- [45] T. Schwetz and J. Zupan, *Journal of Cosmology and Astroparticle Physics* **2011**, 008 (2011).
- [46] B. J. Scholz, A. E. Chavarria, J. I. Collar, P. Privitera, and A. E. Robinson, *Phys. Rev. D* **94**, 122003 (2016).
- [47] R. Essig, M. Sholapurkar, and T.-T. Yu, *Phys. Rev. D* **97**, 095029 (2018).
- [48] A. Belyaev, E. Bertuzzo, C. Caniu Barros, O. Eboli, G. Grilli di Cortona, F. Iocco, and A. Pukhov, *Phys. Rev. D* **99**, 015006 (2019).
- [49] W. Chao, M. Jin, and Y.-Q. Peng, arXiv preprint arXiv:2109.14944 (2021).
- [50] K. Petraki, M. Postma, and M. Wiechers, *Journal of High Energy Physics* **2015**, 1 (2015).
- [51] S. Dimopoulos, G. D. Starkman, and B. W. Lynn, *Phys. Lett.* **168**, 145 (1985).
- [52] F. Avignone III, R. Brodzinski, S. Dimopoulos, G. Starkman, A. Drukier, D. Spergel, G. Gelmini, and B. Lynn, *Physical Review D* **35**, 2752 (1987).
- [53] M. Berger, J. Hubbell, S. Seltzer, J. Chang, J. Coursey, R. Sukumar, D. Zucker, and K. Olsen, "Xcom: Photon cross section database (version 1.5). [online]," (2010), <http://physics.nist.gov/xcom>.
- [54] R. Z. Ferreira, M. D. Marsh, and E. Müller, *Physical Review Letters* **128**, 221302 (2022).
- [55] K. Abe *et al.*, *Physics Letters B* **787**, 153 (2018).